Direct Experimental Observation of in situ Dehydrogenation of an Amine-Borane System Using Gas Electron Diffraction

Aliyu M. Ja'O, Sarah L. Masters, Derek A. Wann, Conor D. Rankine, Joao P. F. Nunes, Jean-Claude Guillemin

Direct Experimental Observation of *in situ* Dehydrogenation of an Amine-borane System Using Gas Electron Diffraction

Aliyu M. Ja'o,[1] Sarah L. Masters,[1*] Derek A. Wann,[2] Conor D. Rankine,[2] João P. F. Nunes[2] and Jean-Claude Guillemin[3]

[1] School of Physical and Chemical Sciences, University of Canterbury, Private Bag 4100, Christchurch 8140, New Zealand

[2] Department of Chemistry, University of York, Heslington, York, YO10 5DD, United Kingdom

[3] Univ Rennes, École Nationale Supérieure de Chimie de Rennes, CNRS, ISCR – UMR6226, F-35000 Rennes, France

ABSTRACT: In situ dehydrogenation of azetidine-BH_3, which is a candidate for hydrogen storage, was observed with the parent and dehydrogenated analogue subjected to rigorous structural and thermochemical investigations. The structural analyses utilized gas electron diffraction supported by high-level quantum calculations, whilst the pathway for the unimolecular hydrogen release reaction in the absence and presence of BH_3 as a bifunctional catalyst was predicted at CBS-QB3 level. The catalyzed dehydrogenation pathway has a barrier lower than the predicted B–N bond dissociation energy, hence favoring the dehydrogenation process over the dissociation of the complex. The predicted enthalpy of dehydrogenation at CCSD(T)/CBS level indicates mild reaction conditions would be required for the hydrogen release and that the compound is closer to thermoneutral than the linear amine boranes. The entropy and free energy change for the dehydrogenation process show that the reaction is exergonic, energetically feasible and will proceed spontaneously towards hydrogen release; all important factors for hydrogen storage.

INTRODUCTION

Amine boranes have received considerable attention in the past two decades owing to their application as potential candidates for chemical hydrogen storage.[1-4] Ammonia borane[5-7] (NH_3BH_3) for instance, with a 19.6% w/v gravimetric weight capacity, has been studied extensively[8-15] both in terms of its ability to generate as well as to regenerate hydrogen under mild conditions. It was found to dehydrogenate at a relatively moderate temperature, yielding three equivalents of molecular hydrogen[16-18] via the formation of the unconventional dihydrogen bonds.[19-23] However, establishing an energy-efficient regeneration process has so far limited its application.[8] Substituted derivatives of ammonia borane such as methyl and dimethyl amine boranes have also been considered.[24, 25] Theoretical investigations have found that methyl substitution at the nitrogen centre of ammonia borane drives the dehydrogenation towards being thermoneutral,[26] with the B–N dative bond having higher stability in the substituted amine boranes than that found in ammonia borane itself. Stability of the B–N bond is critical in chemical hydrogen storage applications because, in a situation where the amine borane complex is not stable, dissociation from across the B–N bond will be favoured over dehydrogenation to release hydrogen.[27] A theoretical investigation of the linear amine boranes $MenH_{3-n}N{\cdot}BH_3$ (n = 1–2) attests to the above; here, the linear amine boranes showed the higher stability of the dative B–N bond and lower dehydrogenation enthalpy.[26, 28] The B–N bond dissociation energies (BDE) of the linear amine boranes obtained experimentally were reported to increase with successive methylation at the nitrogen centre (146, 152, and 160 kJ mol^{-1}).[29, 30] A gas electron diffraction (GED) study of the gaseous linear amine boranes reported an increase in the B–N bond distance with an increase in the number of methyl groups attached to the donor atom.[31] Donor-Acceptor bonds' sensitivity to inductive effects has been attributed to the bond's stability and elongation in methyl substituted amine boranes.[32]

Considering the relationship that exists between the structure of the amine boranes and their

dehydrogenation/hydrogenation cycles, it is pertinent, therefore, to understand their molecular structure. Experimental and theoretical investigations of the structures of aliphatic amine boranes have been reported via X-ray diffraction (XRD), microwave spectroscopy (MWS), GED and quantum-chemical calculations.[31, 33-40] GED has not been used to determine the structure of NH_3BH_3 because of its low vapour pressure at room temperature and propensity to decompose at higher temperatures.[16] However, its methyl-substituted derivatives, which have been found to have high stability, as well as its energetics, have been investigated. A MWS study[10] on NH_3BH_3 revealed the existence of a staggered and an eclipsed conformer at 318 K with a B–N distance of 167.22(5) pm but the data obtained were insufficient to determine the preferred geometry in the gas phase. The staggered conformer was later predicted theoretically to be the preferred geometry.[24] The dative B–N bond, in particular, has always been of interest since it was observed that

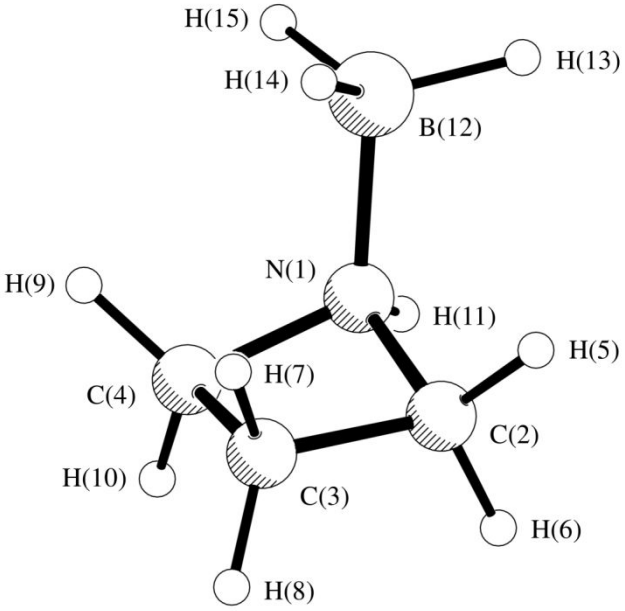

Figure 1: The lowest-energy ground state structure of **A** showing atom numbering.

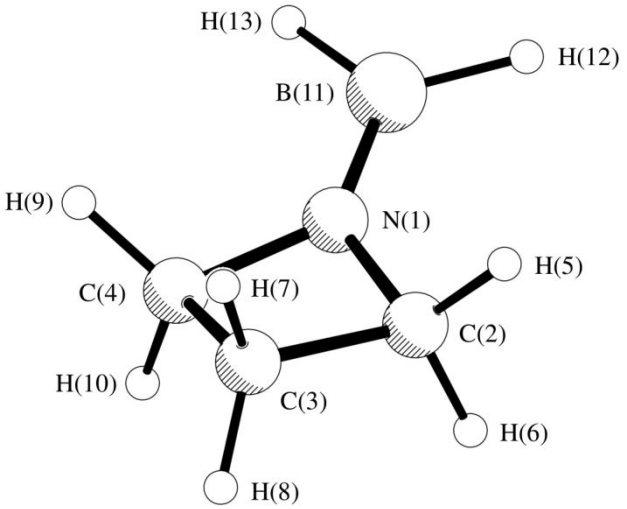

Figure 2: The lowest-energy ground-state structure of **B** (the dehydrogenation product of **A**) showing atom numbering.

dehydrogenation is favoured across this bond.[26] A discrepancy in the B–N distance of trimethylamine borane was observed between an earlier [*r*B–N = 160.9(2) pm][40] and later [*r*B–N = 163.8(1) pm][37] MWS study. This disagreement was attributed to the insufficient microwave data in the former where only one rotation constant (for the ^{14}N isotope species) was obtained, while in each case, the nitrogen atom lies very close to the center of mass which makes it difficult to locate the nitrogen atom. Shibata *et al.*[36] combined GED and MWS to study the structure of trimethylamine borane and obtain a more reliable B–N distance of 165.6(2) pm. This work was conducted after a series of investigations on the halogenated derivatives $(CH_3)_3N{\cdot}BX_3$ (X = F, Cl, Br and I) which found the B–N distances to fall between 165.0 and 167.0 pm.[33-35] Aldridge *et al.* studied the structures of methylamine borane, $CH_3NH_2BH_3$, and dimethylamine borane, $(CH_3)_2NH_2BH_3$, using XRD, GED and quantum-chemical methods.[31] Shortening of the B–N distances was observed in the solid phase [159.36(13) and 159.65(13) pm)] compared to the gas-phase structures [160.2(7) and 161.5(4) pm]. However, the B–N distances from GED have a different physical meaning relative to those obtained by Shibata *et al.* While the former include anharmonic cubic corrections calculated from the third derivatives of the energy ($r_{a3,1}$), the latter include vibrationally-averaged corrections (r_g).[32, 41]

Literature on the molecular structures of the cyclic amine boranes is scant as only aziridine-borane has been investigated as part of an earlier XRD[42] and theoretical[43]

study, and in a later MWS investigation.[44] Cyclic amine boranes should be able to act as electron donors in a push-pull interactions, leading to the release of a hydrogen molecule.[45] Properties associated with the hydrogen storage capabilities of ammonia borane and its cyclic analogues such as aziridine-borane and azetidine-borane were investigated by means of Fourier transform ion cyclotron resonance (FTICR) spectrometry.[45] The cyclic adducts were shown to have hydrogen storage capabilities as a result of the protonation of the amine/boranes which resulted in the formation of dihydrogen. By employing BH_3 as a bifunctional catalyst in the hydrogen release reactions, the reaction pathway for the dehydrogenation of the cyclic amine boranes has also been investigated theoretically.[46, 47]

To broaden our limited knowledge of closely related amine boranes, we have investigated gas-phase structures of the cyclic amine borane azetidine-borane (**A**; Figure 1) and its dehydrogenated counterpart (**B**; Figure 2) via GED coupled with quantum-chemical calculations. We have also investigated the thermochemical properties relating to the hydrogen release reactions. This work represents the first experimental observation of in situ dehydrogenation of an amine-borane system using GED.

EXPERIMENTAL AND COMPUTATIONAL METHODS

Synthesis

A was synthesised using the following procedure adapted from the literature.[44] In a two-necked round-bottomed flask equipped with a stirring bar and a nitrogen inlet, borane-dimethylsulfur complex solution (5 mL of 1 M sol., 5.0 mmol) was slowly added to a cooled (-30 °C) solution of the cyclic amine (0.215 g, 5.0 mmol) in dry dichloromethane (5 mL). The reaction mixture was allowed to warm to room temperature and was stirred for 5 min at this temperature. The solvent was removed *in vacuo* at room temperature. The product was characterised by NMR and IR spectroscopy as well as Mass Spectrometry. Yield: 95%; ^{1}H NMR (CD_2Cl_2, 400 MHz): δ 1.1-1.9 (q, 3H, $^1J_{BH}$ = 89.6 Hz, BH_3), 2.27 (m, 1H, 1 H of NC-CH_2), 2.35 (m, 1H, $^3J_{HH}$ = 7.9 Hz, 1 H of NC-CH_2), 3.37 (quint, $^3J_{HH}$ = 7.9 Hz, 2H of CH_2NCH_2), 3.97 (quint, 2H, $^3J_{HH}$ = $^2J_{HH}$ = 8.5 Hz, 2H of CH_2NCH_2), 5.18 (br, 2H, NH_2); ^{13}C NMR (CD_2Cl_2, 100 MHz): δ 16.8 ($^1J_{CH}$ = 139.8 Hz (t), CH_2CH_2N), 53.3 ($^1J_{CH}$ = 148.2 Hz (t), H_2N); ^{11}B NMR (CD_2Cl_2, 128 MHz): δ = -16.0; IR* (neat, ν): 3242 (m, ν_{NH}), 2971 (w), 2289 (s, ν_{BH}), 1323 (m), 1163 (s), 1027 (m), 936 cm^{-1} (w); HRMS calculated for C_3H_9B-N $[M-1]^+$: 70.0828; found: 70.083.

*Thermo Fisher Scientific IS5FT-IR

Gas Electron Diffraction

GED data were acquired using the University of York gas electron diffractometer[72] An accelerating voltage of around 42.2 keV was used, giving an electron wavelength of approximately 6.0 pm. Electron-sensitive image plates (Fuji BAS-IP MS 2025) were used to record the scattering intensities. Sample/nozzle temperatures, and nozzle-to-image-plate distances and other experimental parameters are given in the SI (Table S1). A flatbed image plate scanner (Fuji BAS-1800II) was used to digitise the scattering intensities. The digitised scattering intensities were reduced to MICs using an azimuthal averaging routine implemented in the University of York data extraction package.[73] The least-squares refinement processes were carried out using the ed@ed program (version 2.3)[74] employing the scattering factors of Ross *et al.*[75] Weighting points for the off-diagonal weight matrices, correlation parameters, and scale factors are given in Table S1.

Computational Methods

All electronic structure calculations were carried out using the GAUSSIAN 09[76] and NWChem[77] software suites. NWChem calculations were carried out using the supercomputing resources of the New Zealand eScience Infrastructure (NeSI). To incorporate the effects of electron correlation on the geometrical parameters, a series of calculations using second-order Møller-Plesset (MP2) perturbation theory[78] and the hybrid meta exchange-correlation functional (M06-2X)[79] were carried out with the 6-31G*, 6-311G*, 6-311+G*,[80-83] and aug-cc-PVTZ[84] basis sets. The convergence of all calculations to minima on the ground-state potential energy surface was verified *via* vibrational frequency analysis. Analytic second derivatives of the energy with respect to nuclear coordinates were calculated at the MP2/6-311+G* level to give the Cartesian force fields which were then used with the SHRINK[54, 85] program to provide estimates of the amplitudes of vibration (*u*) and perpendicular distance corrections (*k*) for use in the GED refinement.

TS structures for the compounds along the dehydrogenation reaction pathways have been obtained using the synchronous transit-guided quasi-Newton (STQN) method.[86] For the BH_3-catalysed reaction pathway, STQN was not used to predict the transition structure because of many molecules on the pathway. The transition structure was obtained by normal eigenvalue-following which follows the reaction path

from the equilibrium geometry to the transition structure by specifying which vibrational mode should lead to a reaction given sufficient kinetic energy. To ascertain the identity of the relevant transition structures, intrinsic reaction coordinate (IRC) calculations[87] were also undertaken at the B3LYP/6-31G* level.

B–N_{BDE} and the thermochemical parameters at 0 and 298.15 K were calculated at CCSD(T)/CBS level and with composite CBS-QB3 method, employing the total atomisation energies and heat of formations as described by Curtiss *et al.*[88] This method predicts thermochemical properties with chemical accuracy with previous tests reported the mean absolute deviation of less than 5.27 kJ mol^{-1}.[71] For CCSD(T)/CBS method, the correlation-consistent aug-cc-pV*n*Z basis sets of Dunning,[52] with *n* = D, T, and Q, have been used to extrapolate the CCSD(T) energies to the complete basis set (CBS) limit by the use of the mixed Gaussian/exponential expression suggested by Peterson *et al*[51] where *n* = 2 (cc-pVDZ), 3 (cc-pVTZ), and 4 (cc-pVQZ).

$$E(n) = E_{CBS} + Be^{-(n-1)} + Ce^{-(n-1)^2} \quad (1)$$

This extrapolation method has been shown to yield atomisation energies in close agreement with experiment as compared to other extrapolation approaches up through *n* = 4.

RESULTS

Quantum Chemical Calculations

The lowest-energy ground-state structure of **A** has a staggered ring conformation with C_s symmetry. The BH_3 group is situated in an axial position on the azetidine ring. The lowest-energy ground-state structure of **B** is also C_s-symmetric, but in this case the BH_2 group lies coplanar with the azetidine ring. The effects of improving the completeness of the basis set and description of electron correlation on the structural parameters has been assessed by a series of calculations at the MP2 level of theory using a range of Pople-type basis sets augmented with additional diffuse and polarisation functions. The results for selected structural parameters are tabulated in Tables 1 and 2; full results from the geometry optimisations are given in the supporting information (SI; Tables S2 and S3). These structural parameters were used to compute the flexible restraints for a SARACEN-type[48-50] GED refinement. For comparison, selected structural parameters for free azetidine (**C**) and azetidine-BH_3 (**A**) are also tabulated in Table 3. Cartesian coordinates for all optimised geometries are given in Tables S6–S14.

Table 1: Optimised structural parameters for **A** at different levels of theory and basis set.

Parameter	MP2/6-31G*	MP2/6-311G*	MP2/6-311+G*	M06-2X/aug-cc-pVTZ
*r*N–B	163.3	162.4	162.4	161.8
*r*N–C	150.5	150.6	150.6	149.9
*r*C···N	213.8	214.2	214.3	214.0
*r*B–H	121.3	121.5	121.6	121.0
*r*C–H	109.1	109.1	109.1	108.6
∠C–N–B	114.6	114.6	114.8	114.1
∠C···N–B	113.4	113.1	113.7	113.9
∠N–B–H	105.0	105.4	105.4	105.3
ϕC–N–B–H	50.6	50.6	50.8	50.6

Distances are in pm and angles and dihedral angles are in °.

Table 2: Optimised structural parameters for **B** at different levels of theory and basis set.

Parameter	MP2/6-31G*	MP2/6-311G*	MP2/6-311+G*	M06-2X/aug-cc-pVTZ
*r*N–B	138.6	138.5	138.7	137.8
*r*N–C	147.6	147.8	147.8	147.1
*r*C···N	211.9	212.0	212.0	212.3
*r*B–H	119.7	119.9	119.9	119.2
*r*C–H	109.4	109.3	109.3	108.8
∠C–N–B	133.9	134.0	134.0	133.7
∠C···N–B	166.5	164.4	163.8	170.5
∠N–B–H	118.7	118.5	118.5	118.6
ϕC–N–B–H	176.1	175.4	175.1	177.3

Distances are in pm and angles and dihedral angles are in °.

Table 3: Main structural differences between azetidine (**C**) and azetidine-BH_3 (**A**).

	Azetidine (**C**)		Azetidine-BH_3 (**A**)
Parameters	GED+MWS	MP2/6-311+G*	MP2/6-311+G*
*r*N–C	147.3(3)	148.6	150.6
*r*C–C	156.3(3)	154.4	154.2

∠C–N–C	91.2(4)	89.4	89.3
∠C–C–C	84.6(4)	85.2	86.7
[a]ϕ	29.7(14)	23.1	17.5

Distances are in pm and angles and dihedral angles are in °.

[a]Ring puckering angle defined as the angle between ∠C–N–C and ∠C–C–C planes

Thermochemical Calculations

The thermochemical properties associated with the hydrogen release reactions, namely the enthalpy (ΔH_r), Gibbs free energy (ΔG_r) and entropy (ΔS_r) along with the dative bond dissociation energy (B-N_{BDE}) are presented in Table 4. These values have been computed at the CCSD(T)/CBS and CBS-QB3 levels of theory. The former method is based on the extrapolation of the energies to the complete basis limit (CBS) using the mixed Gaussian/exponential extrapolation scheme[51] and the correlation-consistent basis sets (cc-pV*n*Z) of Dunning[52] up to the quadruple level. The calculated energies and thermochemical corrections used to determine the thermochemical parameters are given in Tables S15-16.

Table 4: Thermochemical parameters predicted at 298 K at the CCSD(T) and CBS-QB3 levels of theory.

Property	CCSD(T)/CBS	CBS-QB3
B–N_{BDE}	+161.2	+159.2
ΔH_r	–3.4	–5.2
ΔG_r	–38.3	–45.0
ΔS_r	+117.0	+133.5

Units in kJ mol^{-1} except ΔS_r which is in J K^{-1} mol^{-1}.

GED Refinements

The starting parameters for r_{h1}-type least-squares refinements[53] were taken from theoretical geometries optimised at the MP2/6-311+G* level for **A** and **B**. Parameterised molecular models describing **A** and **B + H_2** independently were programmed in FORTRAN90 using 17 independent parameters (six bond lengths, eight bond angles and three dihedral angles) for **A** and 16 independent parameters (six bond lengths, seven bond angles and three dihedral angles) for **B + H_2**. A theoretical Cartesian force field was obtained at the MP2/6-311+G* level and converted into a force field described by a set of symmetry coordinates using the SHRINK program,[54, 55] which generated both amplitudes of vibration (u_{h1}) and the curvilinear corrections (k_{h1}) of r_{h1}-type.[56] All relevant geometric parameters and vibrational amplitudes were then refined. Flexible restraints were employed during the refinements using the SARACEN method.[48-50] The success of the least-squares refinements can be evaluated qualitatively on inspection of the radial-distribution curves (RDC) for **A** and **B + H_2**, reproduced in Figures 3 and 4, respectively (the molecular-scattering intensity curves (MICs) are reproduced in Figures S1 and S2), and quantitatively by inspection of the *R* factors. The R_G factors for the refinements of **A** and **B + H_2** were 15.0% and 8.6%, respectively. Refined structural parameters for **A** and **B + H_2** are provided in Tables S4-S5. Calculated and refined amplitudes of vibration for each atomic pair are provided in Tables S17 and S18 for **A** and **B + H_2** respectively while the least-squares correlation matrix for the refinement of both **A** and **B + H_2** are shown in Tables S19 and S20.

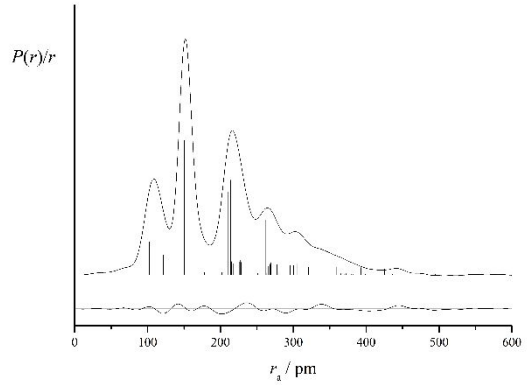

Figure 3: Experimental RDC and difference (experimental minus theoretical) RDC for the least-squares refinement of **A**. Before Fourier inversion, the data were multiplied by $s \cdot \exp(-0.00002s^2)/(Z_C - f_C)(Z_N - f_N)$.

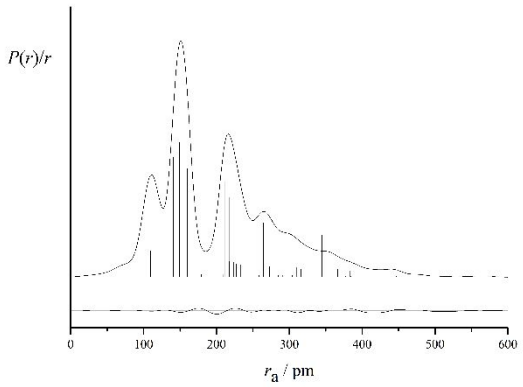

Figure 4: Experimental RDC and difference (experimental minus theoretical) RDC for the least-squares refinement of **B**. Before Fourier inversion, the data were multiplied by $s \cdot \exp(-0.00002s^2)/(Z_C - f_C)(Z_N - f_N)$.

DISCUSSION

This study initially set out to investigate the structure of **A** using gas-phase techniques, however, serendipitously we ended up with the result that **B + H_2** was actually interrogated in the electron beam. This has allowed us to analyse the structure of the dehydrogenated species **B** as well as investigate the thermochemical parameters and reaction pathways for the uncatalysed and catalysed dehydrogenation of **A**.

For the GED analysis of the data the least-squares refinement employed the SARACEN method in which flexible restraints computed from the above calculations were applied to most of the parameters. For **A**, restraints were applied to all 17 geometric parameters while for **B + H_2** restraints were applied to only 10 of the 16 parameters. *r*H–H in the refinement of **B + H_2** was not refined because interatomic distances involving light atoms such as H are known to be poorly defined in the experimental data.[50] As can be seen on inspection of the RDC (Figs. 3 and 4), the experimental and theoretical data for **B + H_2** show a much greater level of agreement compared to **A**. There are several important distinctions between the structures of **A** and **B** that enable us to have confidence in the fit of the model for **B + H_2** to the experimental data. In particular, while the B–N interaction in **A** [162.7(6) pm] is dative, it is covalent in **B**, and is consequently associated with a shorter distance of 140.7(8) pm. Another distinction in the structures of **A** and **B** is the widening of ∠C···N–B from **A** [115.3(4)°] to **B** [162.8(9)°] which can be attributed to the pseudo-planarity of the ···N–BH_2 subunit in **B**; this is a consequence of the lack of a proton on the nitrogen. Examination of the RDC for both these regions reveals a much better fit to the theoretical data for **B + H_2**, and a mismatch for **A**. This leads us to conclude that **A** is not observed in significant quantities in the gas stream under the conditions of the experiment, having thermally decomposed during the data acquisition to **B** and H_2. Thermal decomposition is assumed to take place below about 393±2 K (the temperature of the experiment) and the driver for decomposition is the dehydrogenation reaction along the dative B–N distance that generates **B** and H_2 in equal proportions. This conclusion is supported by the known thermal decomposition of BH_3NH_3 above 340 K in which BH_2NH_2 and H_2 are among the products that have been identified using mass spectrometry and FTIR spectroscopy.[17] The decomposition products cannot be characterised directly here since the University of York gas electron diffractometer does not have an integrated mass spectrometry unit. Therefore, we have further investigated the dehydrogenation process theoretically; this work is discussed further down. We observe an increase in pressure on exposure of the sample to the vacuum. The baseline pressure of the GED experiments was ca. 1×10^{-6} Torr; with the sample admission valve open ca. 5%, a pressure of ca. 1×10^{-5} Torr was recorded in the diffraction chamber. This is one of the factors that made data acquisition for this (and related) sample(s) particularly challenging. The vacuum gauges are located some distance from the point of diffraction, therefore for them to read an order of magnitude higher than the baseline is indicative of a considerable volume of gas entering into the diffraction chamber which we conclude is H_2.

The experimental structure of **C** can only be compared to the predicted structure of **A** since the experimental structure of the latter has not definitively been obtained in this work. Experimental and theoretical investigations[57-65] on the structure of **C** revealed the equatorial conformer having C_s symmetry as the most stable, with the coupling of ring puckering and N–H inversion dominating the structural analysis. Compared to our calculated structure of **A**, the geometry of **C** in the gas phase changes slightly upon complexation with the BH_3 group. The main structural differences between them are shown in Table 3. By employing MWS, the authors in the above investigations measured the rotational transitions of the vibrational ground and excited states of the ring puckering mode. A combination of GED and MWS techniques provided the most reliable structure of **C**, revealing a puckering angle (ϕ) of 29.7(14)° which is significantly wider than that of **A** (17.5°) calculated at MP2/6-311G* level. A similar study

by the above methods for *N*-chloroazetidine[66] revealed almost identical geometries to those of **C**. However, the puckering angle of 32.4(17)° is slightly wider than that of **C**. The narrowing of the puckering angle upon complexation with BH_3 may be attributed to the electron charge transfer between **C** and BH_3.

The calculated structures were found to be generally independent of the level of theory and basis set used, with parameters generally varying by less than 1 pm in the case of the bond lengths or 1° for the angles. An exception to this is a deviation of 1.5 pm for the B–N distance in **A** between MP2/6-31G* and M06-2X/aug-cc-pVTZ. However, in **A**, significant variations can be seen in angles ∠C···N–B and ϕC–N–B–H. ∠C···N–B differed by 2.1 to 2.7° with basis set at the MP2 level and 4.0 to 6.7° between the MP2 and M06-2X calculations. ϕC–N–B–H on the other hand only differed by 1.2 to 2.2° between the MP2 and M06-2X calculations.

The reaction pathways for the uncatalysed and catalysed dehydrogenation of **A** are shown in Fig. 5. The transition-state (TS) structures of the species involved in the dehydrogenation process are depicted in Figures 6 and 7. As can be seen from Figure 5, the condensation reaction between **A** and BH_3 leads to the formation of adduct A---BH_3. The adduct (A---BH_3), having a single bridging B–H–B bond, is more stable than the reactants (**A** and BH_3) by 89.1 kJ mol^{-1}. The adduct then passes through the transition state forming TSA---BH_3 (**TS2**) and proceeds to form **B** and BH_3. This catalytic dehydrogenation pathway has a barrier of 40.1 kJ mol^{-1} compared to the reactants; this is lower than B–N_{BDE} (Table 4) and also lower than it otherwise is in the absence of BH_3 as a catalyst (**TS1**); as such, the dehydrogenation process will be favoured over the dissociation of **A**. The enthalpy, Gibbs free energy and entropy of dehydrogenation values given in Table 4 strengthen this assertion. Hence, BH_3 plays a significant catalytic role as a bifunctional catalyst in the dehydrogenation of **A** to form **B**. This rationale was previously used to explain the dehydrogenation of AlH_3NH_3 and BH_3NH_3 where the Lewis acids BH_3, AlH_3 and GaH_3 acted as bifunctional catalysts.[27, 67, 68]

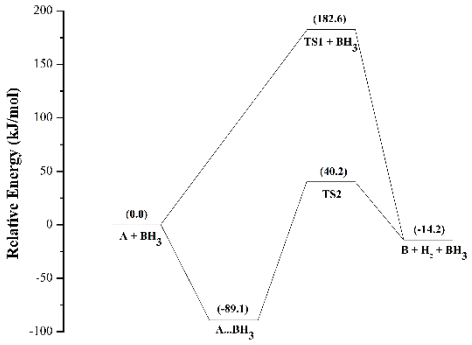

Figure 5: Energy profile for the dehydrogenation of **A** without (via **TS1**) and with (via **TS2**) the presence of catalytic BH_3 at 298.15 K at the CBS-QB3 level. Relative energies are given in kJmol^{-1}.

For the successful implementation of chemical hydrogen storage, the dehydrogenation process should be as close as possible to thermoneutral, thus minimising the heat that is being absorbed or released.[26] As shown in Table 4, the enthalpy of the dehydrogenation process for **A** is almost thermoneutral, indicating the potential of this complex as a recyclable hydrogen storage material. The dehydrogenation reaction is closer to thermoneutral than ammonia borane and dimethylamine borane, for which the dehydrogenation reaction enthalpies at CCSD(T)/CBS level are –21.3 kJ mol^{-1} [69] and –7.5 kJ mol^{-1}.[26] The ΔG_r value at the CCSD(T)/CBS level is comparable to that calculated for aziridine-BH_3 (–35.8 kJ mol^{-1}) at B3LYP/aug-cc-pVTZ level[70] while the ΔS_r is slightly lower than

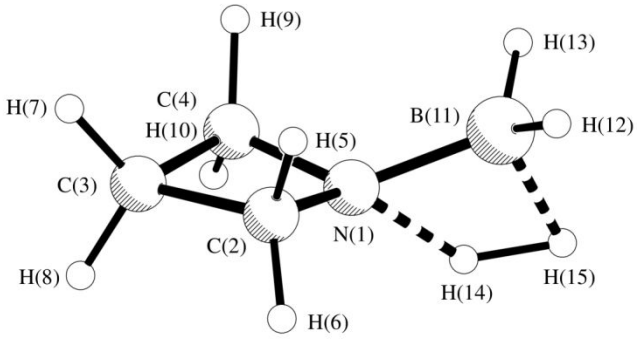

Figure 6: The transition-state structure for the dehydrogenation of **A** in the absence of BH_3 catalyst (**TS1**).

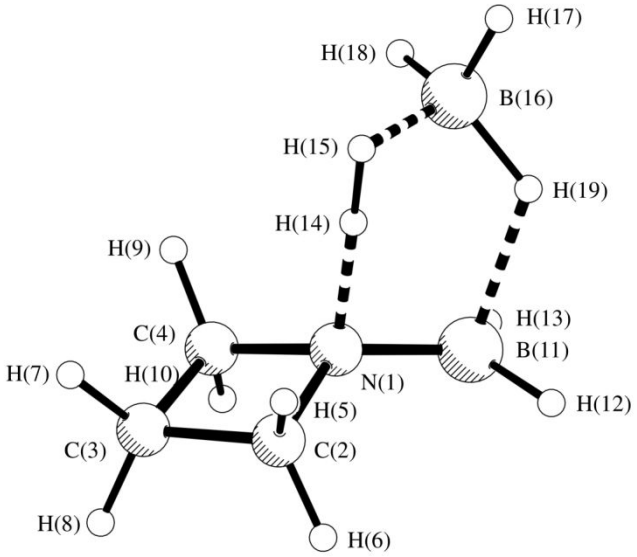

Figure 7: The transition-state structure for the dehydrogenation of **A** in the presence of BH_3 catalyst (**TS2**).

that calculated for NH_3BH_3 (+125.0 J K^{-1} mol^{-1}) at MP2/cc-pVTZ level.[71]

The entropy and free energy change for the dehydrogenation of **A** shows that the reaction is exergonic, energetically feasible and will proceed spontaneously in the forward direction to form **B** and H_2 under standard conditions. The theoretical $B–N_{BDE}$ at both CCSD(T)/CBS and CBS-QB3 levels are higher than the experimental values for NH_3BH_3 {130.1(1) kJ mol^{-1}} and $(CH_3)_2NHBH_3$ {152.3(1) kJ mol^{-1}},[29] indicating a stronger B–N bond in **A** compared to the above compounds.

CONCLUSIONS

The gas electron diffraction data collected were initially intended for the structural study of **A** but, upon careful evaluation, was revealed to contain the dehydrogenated species. Theoretical data for the hydrogenated and dehydrogenated species were obtained at different levels of theory. To support the diffraction data, the calculated structures were used as flexible restraints in the refinements using the SARACEN method. The calculated structures are in good agreement with those reported in the literature for similar compounds by both experimental and theoretical investigation. Small variations in the bond distances and angles of the complexes have been observed by comparing them with their corresponding cyclic amines. The transition structures along the dehydrogenation reaction pathway revealed the formation of dihydrogen bonds which are key to hydrogen release in hydrogen storage compounds. The barriers to the dehydrogenation reactions were comparable to those found for NH_3BH_3 and $(CH_3)_2HNBH_3$. The predicted B–N bond dissociation energy is higher than the experimental value for NH_3BH_3. The enthalpies of dehydrogenation indicate improved thermodynamics (minimum heat required for hydrogen release) and that the compound is closer to thermoneutrality than linear amine boranes studied in earlier work. These observations show that azetidine-BH_3 will serve as a potential candidate for chemical hydrogen storage and its study is worth pursuing.

ASSOCIATED CONTENT

Supporting Information

The supporting information contains the experimental parameters for the GED data collection, reduction and refinement of **B + H_2**, optimised and refined geometric parameters for **A** and **B + H_2**, calculated Cartesian coordinates at different levels of theory for all the molecules involved, energies and corrections for the thermochemical calculations and the molecular intensity curves for **A** and **B + H_2**, calculated and refined amplitudes of vibration for each atomic pair in **A** and **B + H_2** as well as the least-squares correlation matrix for the refinement of **A** and **B + H_2** respectively.

AUTHOR INFORMATION

Corresponding Author

*sarah.masters@canterbury.ac.nz

Author Contributions

J.-C.G. and S.L.M conceived the project, and S.L.M directed the project. A.M.J. synthesised the parent compound, ran the QM calculations and assisted with GED data collection. D.A.W., C.D.R. and J.P.F.N. ran the GED experiments. A.M.J. and S.L.M. drafted the manuscript and all authors contributed significantly to the final manuscript.

Notes

The authors declare no competing financial interest.

ACKNOWLEDGEMENTS

We thank Dr Matthew Polson and Dr Marie Squire for their assistance with synthesis and NMR studies, the Dumont d'Urville exchange for funding the exchange between J.-C.G. and S.L.M. D.A.W and C.D.R thank the

EPSRC for funding the gas electron diffraction and theoretical research at the University of York, UK, for funding a fellowship for D.A.W. (EP/I004122), and for funding the studentship of C.D.R. A.M.J would also like to thank the Federal University Kashere (Nigeria) for funding his doctoral fellowship through the Tertiary Education Trust Fund (TETFund).

REFERENCES

1. Staubitz, A.; Robertson, A. P.; Manners, I. Ammonia-borane and related compounds as dihydrogen sources. *Chem. Rev.* **2010,** *110*, 4079-4124.
2. Hügle, T.; Kühnel, M. F.; Lentz, D. Hydrazine borane: a promising hydrogen storage material. *J. Am. Chem. Soc.* **2009,** *131*, 7444-7446.
3. Singh, S. K.; Zhang, X.-B.; Xu, Q. Room-temperature hydrogen generation from hydrous hydrazine for chemical hydrogen storage. *J. Am. Chem. Soc.* **2009,** *131*, 9894-9895.
4. Staubitz, A.; Sloan, M. E.; Robertson, A. P. M.; Friedrich, A.; Schneider, S.; Gates, P. J.; Schmedt auf der Günne, J.; Manners, I. Catalytic dehydrocoupling/dehydrogenation of N-methylamine-borane and ammonia-borane: synthesis and characterization of high molecular weight polyaminoboranes. *J. Am. Chem. Soc.* **2010,** *132*, 13332-13345.
5. Lippert, E. L.; Lipscomb, W. N. The structure of H_3NBH_3. *J. Am. Chem. Soc.* **1956,** *78*, 503-504.
6. Hughes, E. W. The crystal structure of ammonia-borane, H_3NBH_3. *J. Am. Chem. Soc.* **1956,** *78*, 502-503.
7. Shore, S. G.; Parry, R. W. The crystalline compound ammonia-borane, 1 H_3NBH_3. *J. Am. Chem. Soc.* **1955,** *77*, 6084-6085.
8. Stephens, F. H.; Pons, V.; Baker, R. T. Ammonia–borane: the hydrogen source par excellence? *Dalton Trans.* **2007,** (25), 2613-2626.
9. Umegaki, T.; Yan, J.-M.; Zhang, X.-B.; Shioyama, H.; Kuriyama, N.; Xu, Q. Boron-and nitrogen-based chemical hydrogen storage materials. *Int. J. Hydrogen Energy* **2009,** *34*, 2303-2311.
10. Thorne, L.; Suenram, R.; Lovas, F. Microwave spectrum, torsional barrier, and structure of BH_3NH_3. *J. Chem. Phys.* **1983,** *78*, 167-171.
11. Keaton, R. J.; Blacquiere, J. M.; Baker, R. T. Base metal catalyzed dehydrogenation of ammonia− borane for chemical hydrogen storage. *J. Am. Chem. Soc.* **2007,** *129*, 1844-1845.
12. Denney, M. C.; Pons, V.; Hebden, T. J.; Heinekey, D. M.; Goldberg, K. I. Efficient catalysis of ammonia borane dehydrogenation. *J. Am. Chem. Soc.* **2006,** *128*, 12048-12049.
13. Bluhm, M. E.; Bradley, M. G.; Butterick, R.; Kusari, U.; Sneddon, L. G. Amineborane-based chemical hydrogen storage: enhanced ammonia borane dehydrogenation in ionic liquids. *J. Am. Chem. Soc.* **2006,** *128*, 7748-7749.
14. Conley, B. L.; Guess, D.; Williams, T. J. A robust, air-stable, reusable ruthenium catalyst for dehydrogenation of ammonia borane. *J. Am. Chem. Soc.* **2011,** *133* (36), 14212-14215.
15. Himmelberger, D. W.; Yoon, C. W.; Bluhm, M. E.; Carroll, P. J.; Sneddon, L. G. Base-promoted ammonia borane hydrogen-release. *J. Am. Chem. Soc.* **2009,** *131*, 14101-14110.
16. Hu, M.; Geanangel, R.; Wendlandt, W. The thermal decomposition of ammonia borane. *Therm. Acta.* **1978,** *23*, 249-255.
17. Baitalow, F.; Baumann, J.; Wolf, G.; Jaenicke-Rößler, K.; Leitner, G. Thermal decomposition of B–N–H compounds investigated by using combined thermoanalytical methods. *Therm. Act.* **2002,** *391*, 159-168.
18. Bowden, M.; Autrey, T.; Brown, I.; Ryan, M. The thermal decomposition of ammonia borane: A potential hydrogen storage material. *Curr. Appl. Phys.* **2008,** *8*, 498-500.
19. Richardson, T.; de Gala, S.; Crabtree, R. H.; Siegbahn, P. E. Unconventional hydrogen bonds: Intermolecular BH....HN interactions. *J. Am. Chem. Soc.* **1995,** *117*, 12875-12876.
20. Chen, X.; Bao, X.; Zhao, J.-C.; Shore, S. G. Experimental and computational Study of the formation mechanism of the diammoniate of diborane: the role of dihydrogen bonds. *J. Am. Chem. Soc.* **2011,** *133*, 14172-14175.
21. Klooster, W. T.; Koetzle, T. F.; Siegbahn, P. E. M.; Richardson, T. B.; Crabtree, R. H. Study of the N−H···H−B dihydrogen bond including the crystal structure of BH_3NH_3 by neutron diffraction. *J. Am. Chem. Soc.* **1999,** *121*, 6337-6343.
22. Welch, G. C.; Stephan, D. W. Facile heterolytic cleavage of dihydrogen by phosphines and boranes. *J. Am. Chem. Soc.* **2007,** *129*, 1880-1881.
23. Custelcean, R.; Jackson, J. E. Topochemical control of covalent bond formation by dihydrogen bonding. *J. Am. Chem. Soc.* **1998,** *120*, 12935-12941.
24. Sun, C.; Yao, X.; Du, A.; Li, L.; Smith, S.; Lu, G. Computational study of methyl derivatives of ammonia borane for hydrogen storage. *Phys. Chem. Chem. Phys.* **2008,** *10*, 6104-6106.

25. Bowden, M. E.; Brown, I. W.; Gainsford, G. J.; Wong, H. Structure and thermal decomposition of methylamine borane. *Inorg. Chim. Act.* **2008,** *361*, 2147-2153.
26. Grant, D. J.; Matus, M. H.; Anderson, K. D.; Camaioni, D. M.; Neufeldt, S. R.; Lane, C. F.; Dixon, D. A. Thermochemistry for the dehydrogenation of methyl-substituted ammonia borane compounds. *J. Phys. Chem. A.* **2009,** *113*, 6121-6132.
27. Nguyen, M. T.; Nguyen, V. S.; Matus, M. H.; Gopakumar, G.; Dixon, D. A. Molecular mechanism for H_2 release from BH_3NH_3, including the catalytic role of the lewis acid BH_3. *J. Phys. Chem. A.* **2007,** *111*, 679-690.
28. Umeyama, H.; Morokuma, K. Molecular orbital studies of electron donor-acceptor complexes. 3. Energy and charge decomposition analyses for several strong complexes: carbon monoxide-borane, ammonia-borane, methylamine-borane, trimethylamine-borane, and ammonia-boron trifluoride. *J. Am. Chem. Soc.* **1976,** *98*, 7208-7220.
29. Haaland, A. Covalent versus dative bonds to main group metals, a useful distinction. *Ang. Chem. Int. Ed.* **1989,** *28*, 992-1007.
30. McCoy, R.; Bauer, S. Energetics of the Boranes. I. The heats of reaction of diborane with the methylamines, and of tetramethyldiborane with trimethylamine; the dissociation energy of diborane1. *J. Am. Chem. Soc.* **1956,** *78*, 2061-2065.
31. Aldridge, S.; Downs, A. J.; Tang, C. Y.; Parsons, S.; Clarke, M. C.; Johnstone, R. D.; Robertson, H. E.; Rankin, D. W.; Wann, D. A. Structures and aggregation of the methylamine−borane molecules, $Me_nH_{3-n}N{\cdot}BH_3$(n= 1−3), studied by X-ray diffraction, gas-phase electron diffraction, and quantum chemical calculations. *J. Am. Chem. Soc.* **2009,** *131*, 2231-2243.
32. Hargittai, Rankin, D. W. H. In Stereochemical Applications of gas-phase electron diffraction; Hargittai, I., Hargittai, M., Eds.; VCH Publishers Inc.: New York, United States of America, 1988.
33. Iijima, K.; Shibata, S. Molecular structure and internal rotation of trimethylamine-boron trifluoride. A combination of electron diffraction and spectroscopic data. *Bull. Chem. Soc. Japan.* **1979,** *52*, 711-715.
34. Iijima, K.; Shibata, S. Molecular structures of complexes of trimethylamine with boron trichloride and boron tribromide as determined by gas electron diffraction. *Bull. Chem. Soc. Japan.* **1980,** *53*, 1908-1913.
35. Iijima, K.; Shibata, S. The molecular structure of trimethylamine-boron triiodide as studied by gas electron diffraction. *Bull. Chem. Soc. Japan.* **1983,** *56*, 1891-1895.
36. Iijima, K.; Adachi, N.; Shibata, S. Molecular structure of trimethylamine-borane as studied from gas electron diffraction and spectroscopic data. *Bull. Chem. Soc. Japan.* **1984,** *57*, 3269-3273.
37. Cassoux, P.; Kuczkowski, R. L.; Bryan, P. S.; Taylor, R. C. Microwave spectra of trimethylamine-borane. Boron-nitrogen distance and molecular dipole moment. *Inorg. Chem.* **1975,** *14*, 126-129.
38. Hargittai, M.; Hargittai, I. Electron diffraction investigation of the molecular structures of two trimethylamine-boron halide adducts in the vapour phase. *J. Mol. Struct.* **1977,** *39*, 79-89.
39. Clippard, P. H.; Hanson, J. C.; Taylor, R. C. Crystal and molecular structures of three trimethylamine-boron halide adducts: $(CH_3)_3NBCl_3$, $(CH_3)_3NBBr_3$, and $(CH_3)_3NBI_3$. *J. Cryst. Mol. Struct.* **1971,** *1*, 363-371.
40. Durig, J. R.; Li, Y. S.; Odom, J. D. Microwave spectrum, structure and dipole moment of trimethylamine-borane. *J. Mol. Struct.* **1973,** *16*, 443-450.
41. McCaffrey, P. D.; Mawhorter, R. J.; Turner, A. R.; Brain, P. T.; Rankin, D. W. H. Accurate equilibrium structures obtained from gas-phase electron diffraction data: Sodium chloride. *J. Phys. Chem. A.* **2007,** *111*, 6103-6114.
42. Ringertz, H. The crystal and molecular structure of aziridine borane. *Acta Chem. Scand.* **1969,** *23*, 137443.
43. Kroll, J. A.; Shillady, D. D. Electronic structure of aziridine-borane. *J. Am. Chem. Soc.* **1973,** *95*, 1422-1425.
44. Konovalov, A.; Møllendal, H.; Guillemin, J.-C. Microwave spectrum, structure, barrier to internal rotation, and dipole moment of the aziridine-borane complex ($C_2H_5N{-}BH_3$). *J. Phys. Chem. A.* **2009,** *113*, 8337-8342.
45. Abboud, J. L. M.; Németh, B.; Guillemin, J. C.; Burk, P.; Adamson, A.; Nerut, E. R. Dihydrogen generation from amine/boranes: synthesis, FT-ICR, and computational studies. *Chem. Eur. J.* **2012,** *18*, 3981-3991.
46. Banu, T.; Sen, K.; Ghosh, D.; Debnath, T.; Das, A. K. Cyclic amine-borane adducts as chemical hydrogen storage systems: a computational analysis. *RSC Adv.* **2014,** *4*, 1352-1361.
47. Sen, K.; Banu, T.; Debnath, T.; Ghosh, D.; Das, A. K. Catalytic role of borane and alane in hydrogen release from cyclic amine adducts $C_nH_{2n+1}N{\cdot}XH_3$ [X = B, Al; n = 2–5]: a theoretical interpretation. *RSC Adv.* **2014,** *4*, 21924.
48. Blake, A. J.; Brain, P. T.; McNab, H.; Miller, J.; Morrison, C. A.; Parsons, S.; Rankin, D. W. H.; Robertson, H. E.; Smart, B. A. Structure analysis restrained by *ab initio* calculations: The molecular structure of 2,5-dichloropyrimidine in gaseous and crystalline phases. *J. Phys. Chem.* **1996,** *100*, 12280-12287.

49. Brain, P. T.; Morrison, C. A.; Parsons, S.; Rankin, D. W. H. Tetraborane (10), B_4H_{10}: Structures in gaseous and crystalline phases. *Dalton Trans.* **1996,** (24), 4589-4596.

50. Mitzel, N. W.; Rankin, D. W. SARACEN–molecular structures from theory and experiment: The best of both worlds. *Dalton Trans.* **2003,** (19), 3650-3662.

51. Feller, D.; Peterson, K. A.; Grant Hill, J. On the effectiveness of CCSD (T) complete basis set extrapolations for atomization energies. *J. Chem. Phys.* **2011,** *135*, 044102.

52. Dunning Jr, T. H. Gaussian basis sets for use in correlated molecular calculations. I. The atoms boron through neon and hydrogen. *J. Chem. Phys.* **1989,** *90*, 1007-1023.

53. Atkinson, S. J.; Noble-Eddy, R.; Masters, S. L. Gas-phase structures of ketene and acetic acid from acetic anhydride using very-high-temperature gas electron diffraction. *J. Phys. Chem. A.* **2016,** *120*, 2041-2048.

54. Sipachev, V. Calculation of shrinkage corrections in harmonic approximation. *J. Mol. Struct.: THEOCHEM* **1985,** *121*, 143-151.

55. Sipachev, V. A. Anharmonic corrections to structural experiment data. *Struct. Chem.* **2000,** *11*, 167-172.

56. Wann, D. A.; Less, R. J.; Rataboul, F.; McCaffrey, P. D.; Reilly, A. M.; Robertson, H. E.; Lickiss, P. D.; Rankin, D. W. Accurate gas-phase experimental structures of octasilsesquioxanes ($Si_8O_{12}X_8$; X= H, Me). *Organomet.* **2008,** *27*, 4183-4187.

57. Mastryukov, V. S.; Dorofeeva, O. V.; Vilkov, L. V.; Hargittai, I. Electron diffraction determination of the vapour phase molecular structure of azetidine,$(CH_2)_3NH$. *J. Mol. Struct.* **1976,** *34*, 99-112.

58. Catalán, J.; Mo, O.; Yanez, M. Theoretical study of the structure of azetidine. *J. Mol. Struct.* **1978,** *43*, 251-257.

59. Cremer, D.; Dorofeeva, O. V.; Mastryukov, V. S. Theoretical determination of molecular structure and conformation: Part X. Geometry and puckering potential of azetidine,$(CH_2)_3NH$, combination of electron diffraction and ab initio studies. *J. Mol. Struct.* **1981,** *75*, 225-240.

60. Günther, H.; Schrem, G.; Oberhammer, H. The gas-phase structure of azetidine: Microwave spectroscopy, and electron diffraction and normal coordinate analysis. *J. Mol. Spec.* **1984,** *104*, 152-164.

61. Dutler, R.; Rauk, A.; Sorensen, T. S. A dynamic proton NMR and ab initio MO investigation of the barrier to pyramidal inversion in azetidine. *J. Am. Chem. Soc.* **1987,** *109*, 3224-3228.

62. Dutler, R.; Rauk, A.; Shaw, R. Scaled ab initio force field and vibrational spectra of azetidine. *J. Phys. Chem.* **1990,** *94*, 118-124.

63. Mastryukov, V. S.; Boggs, J. E. Structure and conformation of some saturated four-membered rings, $CH_2CH_2CH_2X$. *J. Mol. Struct.: THEOCHEM* **1995,** *338*, 235-248.

64. López, J. C.; Blanco, S.; Lesarri, A.; Alonso, J. L. Internal dynamics in azetidine: A microwave and ab initio study. *J. Chem. Phys.* **2001,** *114*, 2237-2250.

65. Cremer, D.; Pople, J. General definition of ring puckering coordinates. *J. Am. Chem. Soc.* **1975,** *97*, 1354-1358.

66. Fujiwara, H.; Egawa, T.; Takeuchi, H.; Konaka, S. Molecular structure of N-chloroazetidine studied by gas electron diffraction combined with microwave spectroscopy. *J. Mol. Struct.* **1993,** *301*, 113-123.

67. Nguyen, V. S.; Matus, M. H.; Ngan, V. T.; Nguyen, M. T.; Dixon, D. A. Theoretical study of the hydrogen release from ammonia alane and the catalytic effect of alane. *J. Phys. Chem. C.* **2008,** *112*, 5662-5671.

68. Nguyen, V. S.; Majumdar, D.; Leszczynski, J.; Nguyen, M. T. Hydrogen release from systems containing phosphine, borane, alane and galane: A mechanistic study. *Chem. Phys. Lett.* **2013,** *584*, 30-36.

69. Dixon, D. A.; Gutowski, M. Thermodynamic properties of molecular borane amines and the $[BH_4^-][NH_4^+]$ salt for chemical hydrogen storage systems from *ab initio* electronic structure theory. *J. Phys. Chem. A.* **2005,** *109*, 5129-5135.

70. Németh, B.; Khater, B.; Guillemin, J.-C.; Veszprémi, T. Differences between amine-and phosphine-boranes: synthesis, photoelectron spectroscopy, and quantum chemical study of the cyclopropylic derivatives. *Inorg. Chem.* **2010,** *49*, 4854-4864.

71. Matus, M. H.; Anderson, K. D.; Camaioni, D. M.; Autrey, S. T.; Dixon, D. A. Reliable predictions of the thermochemistry of boron− nitrogen hydrogen storage compounds: $B_xN_xH_y$, x= 2, 3. *J. Phys. Chem. A.* **2007,** *111*, 4411-4421.

72. Rankine, C. D.; Nunes, J. P. F.; Lock Feixas, T.; Young, S.; Wann, D. A. A. The structure of 4-(Dimethylamino) benzonitrile using gas electron diffraction: a new lease of life for the only gas electron diffractometer in the UK. *J. Phys. Chem. A.* **2018,** *122*, 5656-5665.

73. Nunes, J. P. F. Developments towards time-resolved electron diffraction: roadmap to "molecular movies". Ph.D Thesis, University of York, 2017.

74. Hinchley, S. L.; Robertson, H. E.; Borisenko, K. B.; Turner, A. R.; Johnston, B. F.; Rankin, D. W.; Ahmadian, M.;

Jones, J. N.; Cowley, A. H. The molecular structure of tetra-*tert*-butyldiphosphine: an extremely distorted, sterically crowded molecule. *Dalton Trans.* **2004,** (16), 2469-2476.
75. Ross, A. W.; Fink, M.; Hilderbrandt, R. In international tables for crystallography; Wilson, A. J. C., Ed.; Kluwer Academic Publishers: Dordrecht, Netherlands, 1992; Vol. C.
76. Frisc Frisch, M. J.; Trucks, G. W.; Schlegel, H. B.; Scuseria, G. E.; Robb, M. A.; Cheeseman, J. R.; Scalmani, G.; Barone, V.; Mennucci, B.; Petersson, G. A.; et al. Gaussian 09, Revision D.01; Gaussian, Inc.: Wallingford, CT, 2009.
77. Valiev, M.; Bylaska, E. J.; Govind, N.; Kowalski, K.; Straatsma, T. P.; Van Dam, H. J.; Wang, D.; Nieplocha, J.; Apra, E.; Windus, T. L. NWChem: a comprehensive and scalable open-source solution for large scale molecular simulations. *Comp. Phys. Comm.* **2010,** *181*, 1477-1489.
78. Frisch, M. J.; Head-Gordon, M.; Pople, J. A. A direct MP2 gradient method. *Chem. Phys. Lett.* **1990,** *166*, 275-280.
79. Zhao, Y.; Truhlar, D. G. The M06 suite of density functionals for main group thermochemistry, thermochemical kinetics, noncovalent interactions, excited states, and transition elements: two new functionals and systematic testing of four M06-class functionals and 12 other functionals. *Theo. Chem. Acc.* **2008,** *120*, 215-241.
80. Hehre, W. J.; Ditchfield, R.; Pople, J. A. Self-consistent molecular orbital methods. XII. Further extensions of gaussian-type basis sets for use in molecular orbital studies of organic molecules. *J. Chem. Phys.* **1972,** *56*, 2257-2261.
81. Krishnan, R.; Binkley, J. S.; Seeger, R.; Pople, J. A. Self-consistent molecular orbital methods. XX. A basis set for correlated wave functions. *J. Chem. Phys.* **1980,** *72*, 650-654.
82. Francl, M. M.; Pietro, W. J.; Hehre, W. J.; Binkley, J. S.; Gordon, M. S.; DeFrees, D. J.; Pople, J. A. Self-consistent molecular orbital methods. XXIII. A polarization-type basis set for second-row elements. *J. Chem. Phys.* **1982,** *77*, 3654-3665.
83. Frisch, M. J.; Pople, J. A.; Binkley, J. S. Self-consistent molecular orbital methods 25. Supplementary functions for Gaussian basis sets. *J. Chem. Phys.* **1984,** *80*, 3265-3269.
84. Woon, D. E.; Dunning J, T. H. Gaussian basis sets for use in correlated molecular calculations. V. Core-valence basis sets for boron through neon. *J. Chem. Phys.* **1995,** *103*, 4572-4585.
85. Sipachev, V. Local centrifugal distortions caused by internal motions of molecules. *J. Mol. Struct.* **2001,** *567*, 67-72.
86. Peng, C.; Schlegel, H. B. Combining synchronous transit and quasi-newton methods to find transition states. *Israel J. Chem.* **1993,** *33*, 449-454.
87. Gonzalez, C.; Schlegel, H. B. Reaction path following in mass-weighted internal coordinates. *J. Phys. Chem.* **1990,** *94*, 5523-5527.
88. Curtiss, L. A.; Raghavachari, K.; Redfern, P. C.; Pople, J. A. Assessment of Gaussian-2 and density functional theories for the computation of enthalpies of formation. *J. Chem. Phys.* **1997,** *106*, 1063-1079.

ToC Graphic

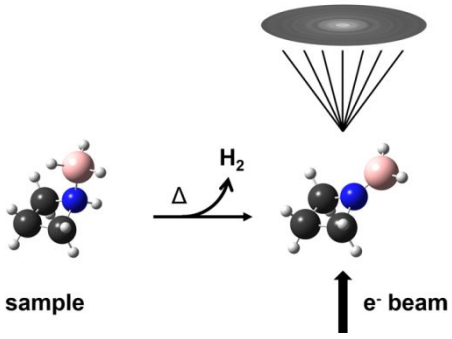

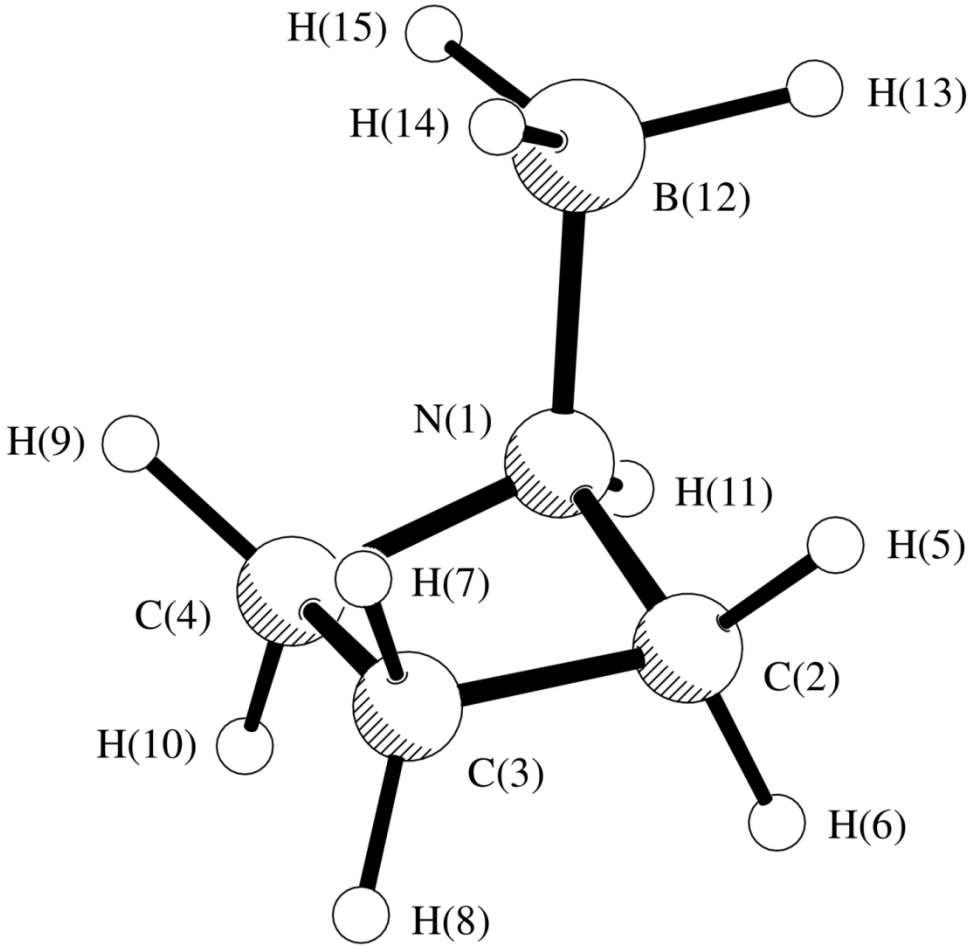

Figure 1: The lowest-energy ground state structure of **A** showing atom numbering.

127x124mm (300 x 300 DPI)

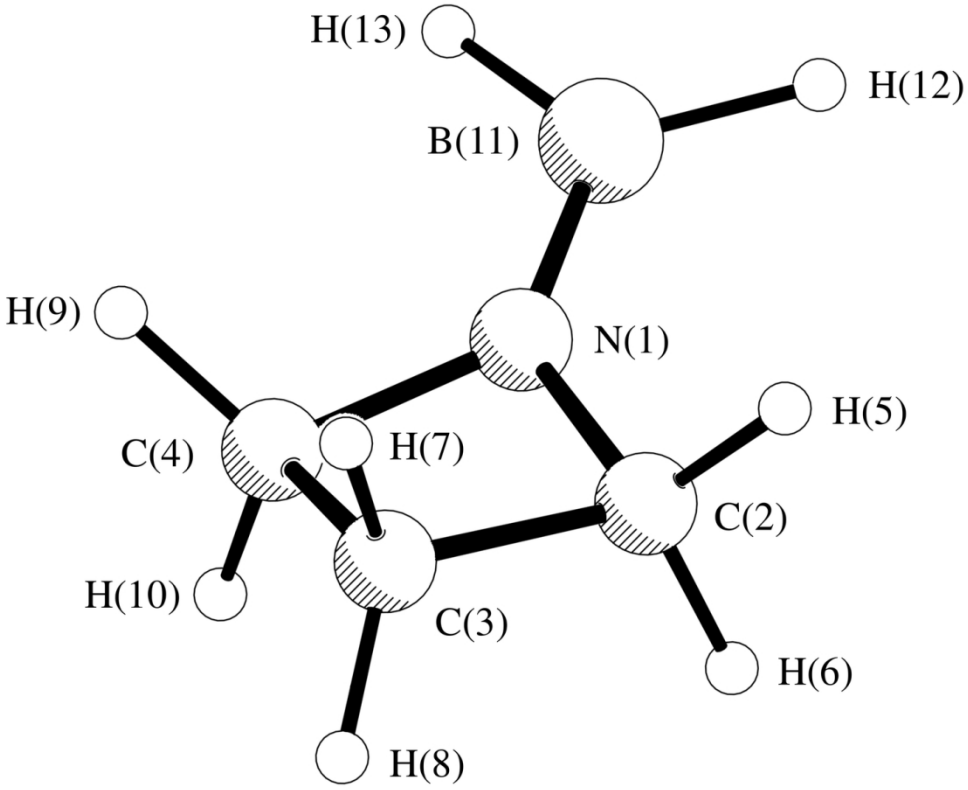

Figure 2: The lowest-energy ground-state structure of **B** (the dehydrogenation product of **A**) showing atom numbering.

127x104mm (300 x 300 DPI)

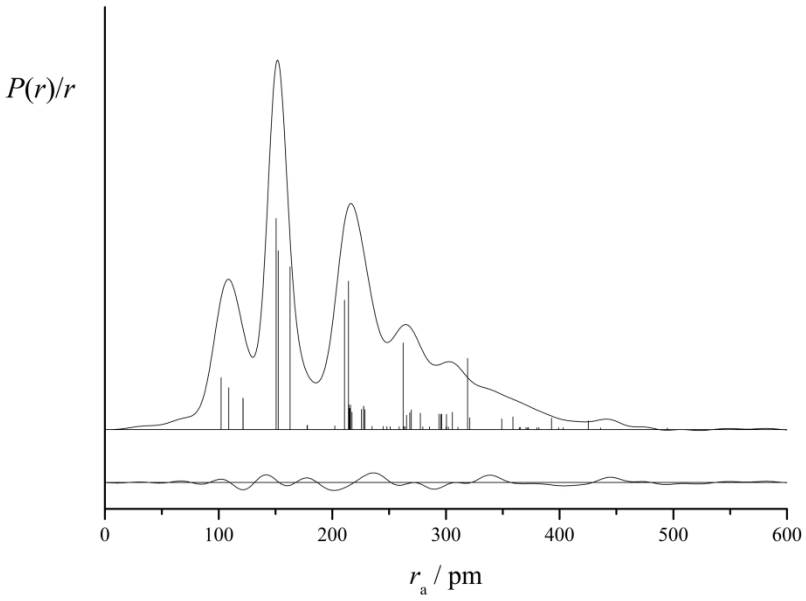

Figure 3: Experimental RDC and difference (experimental minus theoretical) RDC for the least-squares refinement of **A**. Before Fourier inversion, the data were multiplied by $s \cdot \exp(-0.00002 s^2)/(ZC - f_C)(Z_N - f_N)$.

288x201mm (300 x 300 DPI)

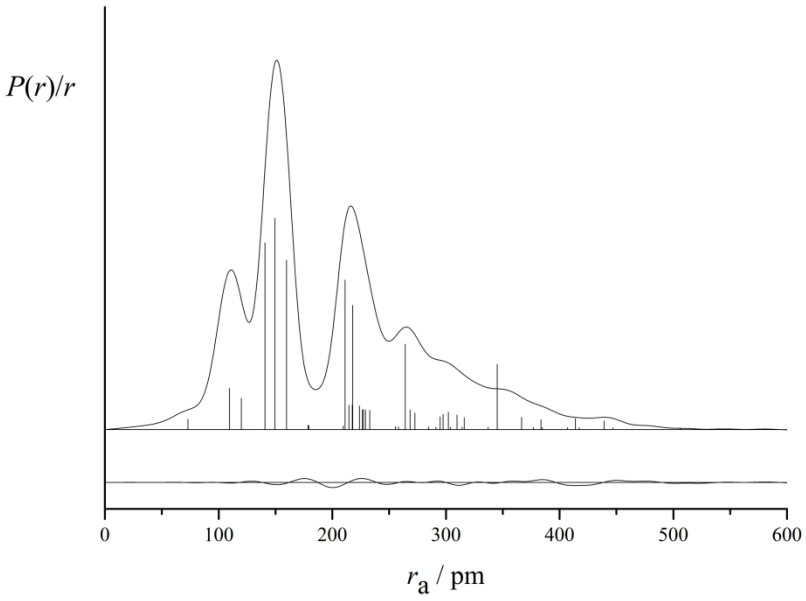

Figure 4: Experimental RDC and difference (experimental minus theoretical) RDC for the least-squares refinement of **B** + H_2. Before Fourier inversion, the data were multiplied by $s \cdot \exp(-0.00002 s^2)/(Z_C - f_{C</sub>))(z_{N</sub>) - f_N)$.

288x201mm (300 x 300 DPI)

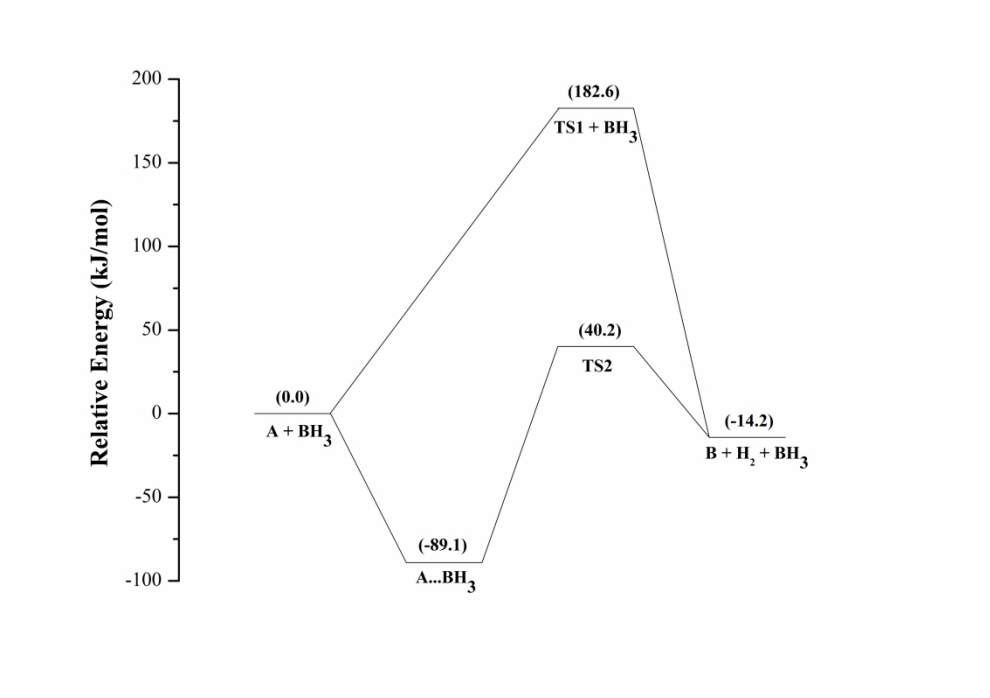

Figure 5: Energy profile for the dehydrogenation of **A** without (via **TS1**) and with (via **TS2**) the presence of catalytic BH_3 at 298.15 K at the CBS-QB3 level. Relative energies are given in $kJmol^{-1}$.

288x201mm (300 x 300 DPI)

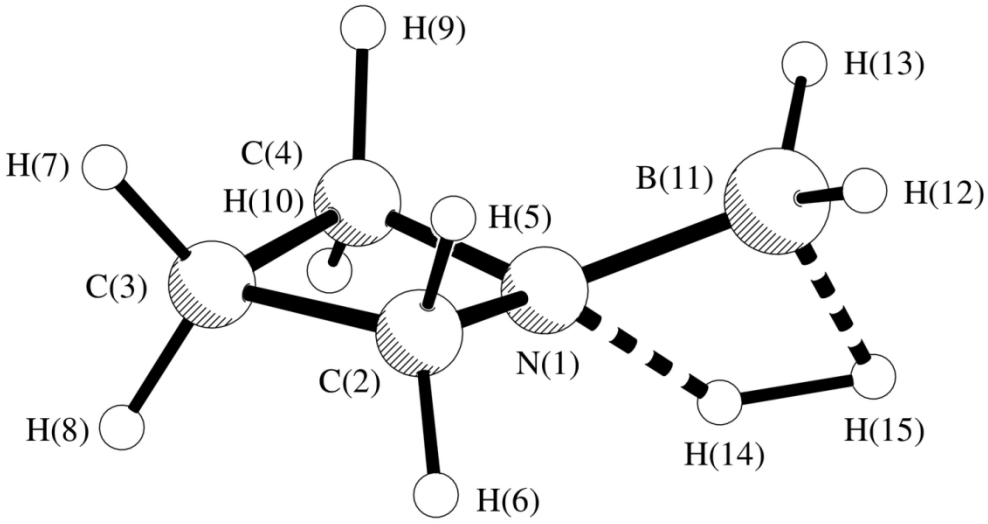

Figure 6: The transition-state structure for the dehydrogenation of **A** in the absence of BH_3 catalyst (**TS1**).

127x69mm (300 x 300 DPI)

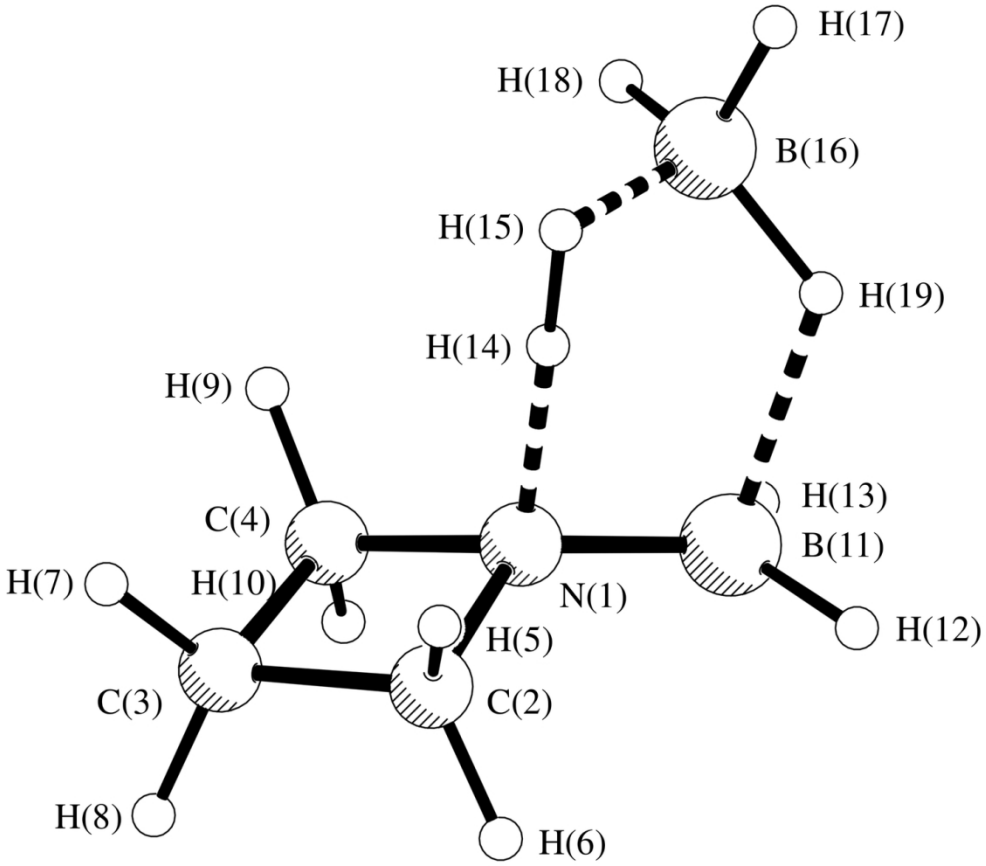

Figure 7: The transition-state structure for the dehydrogenation of **A** in the presence of BH_3 catalyst (**TS2**).

126x112mm (300 x 300 DPI)

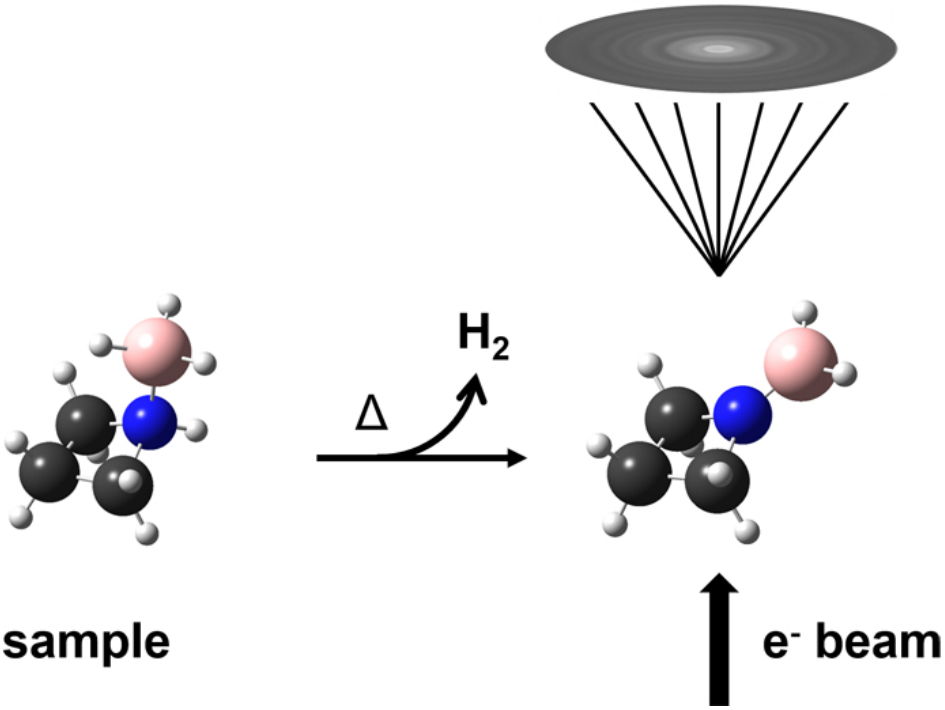

Table of Contents Graphic

62x44mm (300 x 300 DPI)